Biofabrication

International Society for Biofabrication

PAPER

3D printing of HEK 293FT cell-laden hydrogel into macroporous constructs with high cell viability and normal biological functions

To cite this article: Liliang Ouyang *et al* 2015 *Biofabrication* **7** 015010

Biofabrication

RECEIVED
12 September 2014

REVISED
15 December 2014

ACCEPTED FOR PUBLICATION
26 January 2015

PUBLISHED
18 February 2015

PAPER

3D printing of HEK 293FT cell-laden hydrogel into macroporous constructs with high cell viability and normal biological functions

Liliang Ouyang[1,2,6], **Rui Yao**[1,2,6], **Xi Chen**[3,6], **Jie Na**[3] **and Wei Sun**[1,2,4,5]

[1] Biomanufacturing Center, Department of Mechanical Engineering, Tsinghua University, Beijing 100084, People's Republic of China
[2] Biomanufacturing and Rapid Forming Technology Key Laboratory of Beijing, Beijing 100084, People's Republic of China
[3] Center for Stem Cell Biology and Regenerative Medicine, School of Medicine, Tsinghua University, Beijing 100084, People's Republic of China
[4] Biomanufacturing Engineering Research Laboratory, Graduate School at Shenzhen Tsinghua University, Shenzhen 518055, People's Republic of China
[5] Department of Mechanical Engineering, Drexel University, Philadelphia, Pennsylvania 19104, USA
[6] These authors contributed to this work equally.

E-mail: weisun@tsinghua.edu.cn **and** jie.na@tsinghua.edu.cn

Keywords: three dimensional printing, cell viability, signal transduction, Wnt, HEK 293FT

Abstract

3D printing has evolved into a versatile technology for fabricating tissue-engineered constructs with spatially controlled cells and biomaterial distribution to allow biomimicking of *in vivo* tissues. In this paper, we reported a novel study of 3D printing of cell lines derived from human embryonic kidney tissue into a macroporous tissue-like construct. Nozzle temperature, chamber temperature and the composition of the matrix material were studied to achieve high cell viability (>90%) after 3D printing and construct formation. Long-term construct stability with a clear grid structure up to 30 days was observed. Cells continued to grow as cellular spheroids with strong cell–cell interactions. Two transfected cell lines of HEK 293FT were also 3D printed and showed normal biological functions, i.e. protein synthesis and gene activation in responding to small molecule stimulus. With further refinement, this 3D cell printing technology may lead to a practical fabrication of functional embryonic tissues *in vitro*.

1. Introduction

Development of 3D bioprinting technologies can enable novel biomedical researches by creating 3D structures resembling *in vivo* microenvironment and tissue structure [1, 2]. It is now commonly accepted that 2D culture conditions cannot efficiently represent the complex *in vivo* microenvironment [2]. Cells cultured in 2D monolayers were found to display different gene expression and functionality compared to cells in native tissues or 3D culture conditions [3, 4]. Hence, various new technologies were developed to fabricate 3D constructs to explore the cellular behaviors in 3D condition, i.e. cell interaction [5, 6], stem cell differentiation [7–9], vascularization [10, 11] and ossification [12], with the potential application in drug screening [13–16] and regenerative medicine [17–19].

Scaffold-based strategy is a commonly used tissue engineering approach to create 3D structure. However, the seeding efficiency of cells in preformed 3D structures was often poor due to long cell infiltrating distance and suboptimal adhesion conditions. Therefore, it is hard to control cell viability and density within the scaffold. 3D cell-laden printing technology may overcome above problems by pre-mixing cells and biomaterials, then deposit them in desired pattern. Commonly investigated 3D cell printing technology include: laser printing [20, 21], inkjet printing [22, 23], extrusion printing [24], valve-based printing [25] and acoustic cell encapsulation [26]. Cancer cells [27], stem cells [28, 29] and cells derived from adipose tissue [30, 31], cardiac tissue [32, 33], hepatic tissue [34], etc have been printed in cell-laden constructions for different purposes. So far few studies about 3D printing of embryonic tissue derived cells were reported. Shu *et al* applied a valve-based cell printer to print HEK 293 cells with culture media as preliminary experiment [35]. Lee *et al* fabricated 2D patterning of embryonic neural cells onto a 3D multilayered collagen gel to generate artificial neural tissue composites

[36]. However, the long-term growth and key biological functions such as protein synthesis and the responsiveness to biological signal stimulus of 3D printed cells have not been carefully evaluated.

In this study, HEK 293FT cell were used because it is an immortalized cell line derived from human embryonic kidney that has been widely used in biology experiments to study protein biochemistry and cell signaling. It has also been used for mammalian protein production and virus packaging [37, 38]. To examine essential cellular functions of bioprinted cells grown in 3D structure, such as protein synthesis and response to cytokine signaling, we also employed HEK 293FT cells that had been genetically engineered to express Wnt3a protein or carry a Wnt reporter. Wnt signaling pathway plays important function during embryo development, tissue homeostasis and human diseases such as cancer [39]. Wnt3a, a member of the Wnt gene family, is a secreted cytokine that can activate canonical Wnt/β-catenin pathway. Upon receptor binding, Wnt ligands can trigger a cascade of signaling events and lead to the activation of Wnt target genes. To mimic this process, Wnt reporter plasmid was engineered which contains multiple Wnt responsive elements driving the expression of a red fluorescent protein gene mCherry. Upon activation of Wnt signaling, the reporter gene will express, indicating that the corresponding cellular pathway is functional [39]. Using this system in our study will allow easy and accurate analysis of typical cellular function of embryonic cells.

Gelatin, alginate and fibrinogen were selected as the hydrogel materials in this study due to their high biocompatibility with mammalian cells and ease of gelation. The extrusion-based 3D cell printing methodology makes use of the temperature-sensitive gelation property of gelatin to fabricate 3D construct [24]. Alginate is widely used in drug delivery and tissue engineering applications for its structural similarity to the extracellular matrices [40]. Fibrinogen is one of the most abundant plasma proteins and can be crosslinked in physiological condition to stabilize the 3D structure [41]. Based on the pre-crosslinking of gelatin before printing, the adopted continuous bio-printer can build 3D hybrid materials constructs by subsequent crosslinking. Studies on hepatocytes [24], metabolic syndrome [30], *in vitro* angiogenesis [31] and adipose tissue-derived stem cells (ADSCs) differentiation have been carried out using this cell printing technique.

In this study, we reported 3D printing of HEK 293FT cells into cell-laden macroporous constructs via an extrusion-based 3D cell printing machine. Printing parameters were systematically analyzed and optimized to achieve high cell viability and stable 3D structure for up to 30 days. Right after printing, the viability of HEK 293FT and its genetically engineered derivative cell lines, including Wnt3a expressing cells (Wnt3a-293FT) and Wnt reporter cells (Wnt reporter-293FT), reached 92.25, 87.9 and 74.66%, respectively. After 3 days, nearly 100% cells were alive. They proliferated and formed cellular aggregates with the diameter of tens of micrometers. Furthermore, we performed detailed comparison of the cell morphology and the proliferation rate in 2D culture and in 3D cell-laden constructs. Finally, we showed that robust ectopical protein expression and cell signaling pathway activation can be achieved in 3D gel structure compared with that in 2D culture conditions.

2. Materials and methods

2.1. Cell culture

HEK 293FT cells (Invitrogen, Life Technologies, USA) were cultured at 37 °C in 5% CO_2 in high glucose Dulbecco's modified Eagle's medium (H-DMEM, Gibco, Life Technologies, USA) supplemented with 10% fetal bovine serum (FBS) (BI, Israel), 1% GlutaMax-1 (Invitrogen, Life Technologies, USA), 100 U mL^{-1} penicillin and 100 $\mu g\ mL^{-1}$ streptomycin. 0.25% (w/v) trypsin with 0.2% (w/v) ethylene diamin tetra-acetate (EDTA) was used to dissociate and passage cells when cell confluence reached 90%.

Recombinant Wnt3a plasmid CAG-Igk-Wnt3a-Flag-His-IRES-puro was constructed and transfected into HEK 293FT cells to establish Wnt3a-293FT cells. Wnt3a-293FT cells were maintained by selection using 0.5 $\mu g\ mL^{-1}$ puromycin (SIGMA, USA). For Wnt reporter-293FT, a piggyBac plasmid containing 7xTCF/Lef binding sites driving mCherry gene and PGK promoter driving Neomycin resistant gene was transfected into normal HEK 293FT cells. Cells with no background mCherry expression showed strong red fluorescence in respond to CT99021 (a GSK3 inhibitor and Wnt signaling pathway activator) treatment, which were selected by fluorescence-activated cell sorting (FACS) (BD, Aria II, USA). Both Wnt3a-293FT and Wnt reporter-293FT were cultured in the same medium as normal HEK 293FT cells.

2.2. Material preparation

Gelatin (type A, SIGMA, G1890, USA) and sodium alginate (SIGMA, A0682, USA) were dissolved in 0.5% (w/v) sodium chloride solution at the concentration of 20% (w/v) and 4% (w/v), respectively. Both the two solutions were sterilized under 70 °C for 30 min for three times. Sterilized gelatin and sodium alginate solution were stored at 4 °C and warmed up to 37 °C before use. 8% (w/v) fibrinogen solution was prepared by dissolving fibrinogen powders (Sigma, F8630, USA) in H-DMEM at 37 °C and used to suspend cells immediately. Two recipes of cell-laden solutions were tested: gelatin–alginate–fibronogen (G–A–F):10% gelatin, 1% alginate and 2% fibrinogen; gelatin–alginate (G–A):10% gelatin and 1% alginate. For each experiment, cell-laden solutions were prepared immediately before 3D printing. 293FT cells were dissociated to single cells and suspended in fibrinogen

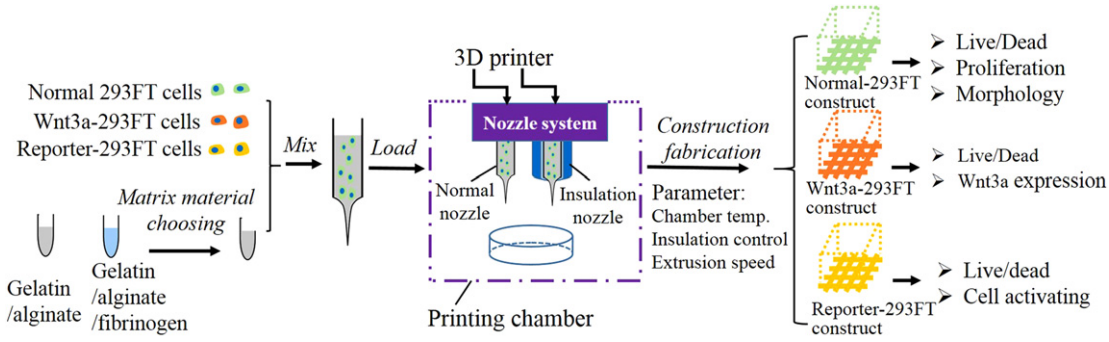

Figure 1. Schematic view of the 3D bioprinting process. Three different kinds of cells and two matrix material configurations were studied. Cells were blended with matrix materials, and then loaded to the printer for printing. Composition of matrix materials and printing parameters were optimized based on the cell viability and structure stability. Cell proliferation and normal biological functions were tested.

solution or culture medium and then gently mixed with G–A solution to reach a final concentration of 2×10^6 cells/mL.

2.3. 3D bioprinting and culture of cell-laden constructs

By using a 3D cell printer developed by our group, we fabricated a macroporous constructs in a layer-by-layer fashion with designed size of 8×8 mm in cross-section and 0.9 mm (six layers) in thickness. Briefly, the cell-laden solution was loaded into a sterilized 1 mL syringe and set in the printer for printing in air. The process parameters, i.e. printing chamber temperature, extrusion speed, and nozzle temperature were optimized in this study. After 3D bioprinting, cell-laden constructs were chemically crosslinked by immersing in 100 mM calcium chloride solution for 3 min to crosslink sodium alginate. For the G–A–F group, 20 U mL^{-1} thrombin (SIGMA, T4648, USA) in phosphate buffer solution (PBS) was used to crosslink fibrinogen. Between each solution addition, the constructs were gently washed for 2–3 times. The G–A/cell constructs were cultured in the same medium as HEK 293FT cells at 37 °C and 5% CO2. The G–A–F/cell constructs were cultured in that medium supplemented with 20 μg aprotinin at 37 °C and 5% CO_2. Each construct was cultured in one 35mm petri dish. 1.5 mL of culture medium were added to each well and changed every 2 days. The schematic view of the process of this process is shown in figure 1.

2.4. Live/dead staining

A fluorescent live/dead staining was used to determine cell viability in the 3D cell-laden constructs according to the manufacturer's instructions. Briefly, samples were gently washed in PBS for 3 times before immersing in staining solution. 1 μM Calcein-AM (SIGMA, USA) and 2 μM propidium iodide (SIGMA, USA) in PBS were used to stain live cells (green) and dead cells (red) for 15 min while avoiding light. Subsequently, samples were washed in PBS for 3 times. A confocal microscope (LSM710META, Zeiss, Germany) was used for image acquisition. Cell viability was determined by count/size tool of Image-Pro-Plus and calculated by dividing the total number of cells by green stained cells. Three different fields were counted for each sample.

2.5. Morphology analysis

To analyze cell morphology in the 3D hydrogel, f-actin filaments and nuclei were stained using FITC-phalloidin and DAPI, respectively. Briefly, 3D cell-laden constructs were fixed with 4% paraformaldehyde for 20 min, and subsequently permeabilized in 0.1% triton X-100 for 30 min and blocked in 1% bovine serum albumin for 30 min. 5 μg mL^{-1} FITC-phalliodin (SIGMA, USA) and 1 μg mL^{-1} DAPI (SIGMA, USA) were successively added to the constructs and incubated in dark for 20 and 5 min, respectively. Between each solution adding, the samples were gently washed with PBS for 3 times. A laser confocal microscope (LSM710META, Zeiss, Germany) was used for image acquisition. Based on the fluorescent images, the diameter of a circle with the same area of the aggregate cross-section was defined as the aggregate diameter, and the cross-section area was determined by count/size tool of Image-Pro-Plus software.

2.6. Cell proliferation assay

Cell Counting Kit-8 (CCK-8, DOJINDO, Japan) was used to examine cell proliferation in 2D cultured samples and in 3D bioprinted constructs according to the manufacturer's instructions. Briefly, 5×10^4 HEK 293 FT cells were seeded in a 35 mm petri dish as the 2D culture sample. 80 μL CCK-8 in 800 μL culture medium was added into each culture dish containing 2D or 3D sample and incubated in the dark for 2 h at 37 °C. After incubation, 110 μL supernatant from 2D or 3D samples were transferred into 96-well plates and the optical density (OD) was read at 450 nm using a microplate reader (BIO-RAD, Model 680, USA) immediately. 3D construct without cells was treated

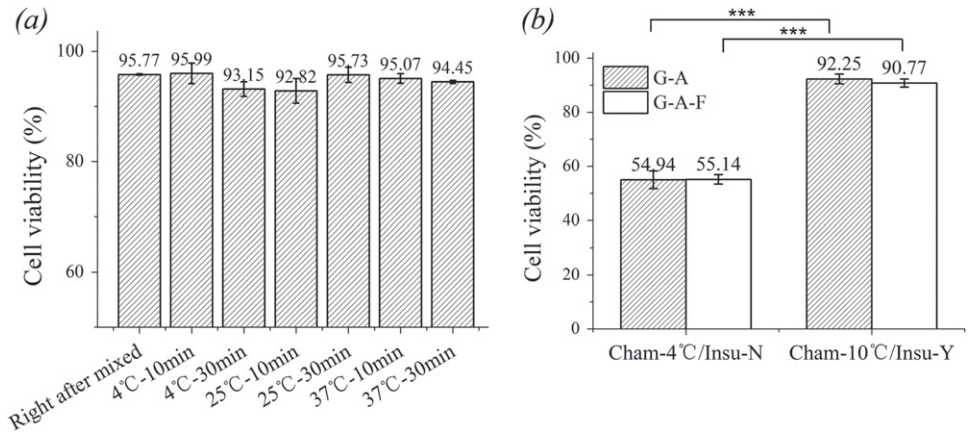

Figure 2. Matrix materials' influence on cell viability. (a) Influence of storing cell-laden gelatin/alginate mixture at 4, 25, and 37 °C for 10 and 30 min on cell viability. (b) Cell viability changed with two printing parameters' configurations for gelatin/alginate (G–A) and gelatin/alginate/fibrinogen (G–A–F) material groups. All the results above were based on HEK 293FT cells.

the same way and CCK-8 medium was used as the blank control. Three samples were tested for each group.

Apart from CCK-8 assay, the growing of cell aggregates was also measured to reflect the proliferation in 3D condition. The volume of aggregate was determined by the function of sphere volume ($V = \pi d^3/6$, V means volume, d means diameter) and then the relative or normalized volume to day 1 was calculated by dividing volume of day 1 by volume of each day. The normalized data of aggregate volume was compared with normalized data of 2D OD value.

2.7. Western blot

Wnt3a protein expression was quantified by western blot. Wnt3a-293FT cells (final concentration 10^7 cells/mL) was 3D printed as described above. 10 h after printing, the culture medium was replaced with DMEM/F12 medium without FBS but supplemented with 0.1 mg L^{-1} heparin (SIGMA, H3149, USA). 48 h later, the supernatant around tissue constructs was removed. The constructs were then dissolved in 55 mM sodium citrate and 20 mM EDTA in 0.9% NaCl and stirred using pipette for 10 min at RT to allow alginate depolymerization and cell isolation. Cells were lysed in RIPA buffer and cell lysates (20 μg total protein per lane) were separated by electrophoresis on a 12% polyacrylamide gel. Then proteins were transferred from the gel onto a nitrocellulose membrane, and blocked for 1 h at RT in TBS containing 5% skimmed milk and 0.1% Tween 20, followed by an overnight incubation at 4 °C with the primary antibody (Mouse anti-Flag-M2 (Sigma), 1/1000 dilution) in the same buffer. Membranes were then incubated with the secondary antibody (goat anti-mouse IgG (HRP-linked) (Jackson), 1/1000 dilution) for 1 h in 1xTBS with 1% skim milk and 0.1% Tween20 at RT. Proteins were detected using ECL + solution (DingGuo) and gel image system (Bio-Rad, Chemi-Doc™ XRS+ System, USA).

2.8. Activation of Wnt reporter in 3D bioprinted constructs

Small molecule Wnt signaling pathway activator CT99021 was used to determine the responsiveness of Wnt reporter-293FT cells. 3 μM CT99021 was added in 2D and 3D culturing dish 24 h after seeding or printing. 48 h later, a fluorescence microscope (Nikon, TiE, Japan) was used to analysis the expression of mCherry. Normal HEK 293FT cell was used as the control group.

2.9. Statistical analysis

All results were presented as the mean ± standard deviation (SD). Statistical analysis was performed using two-way analysis of variance (ANOVA) in conjugation with a Bonferroni post-hoc test and a student t-test in Graphpad Prism. Statistical significance was defined as $^*p < 0.05$, $^{**}p < 0.01$, and $^{***}p < 0.005$. Three independent trials were carried out unless otherwise stated.

3. Results

3.1. Influence of 3D printing parameters on cell viability

As showed in figure 1, HEK 293FT cells, Wnt3a-293FT cells and Wnt reporter-293FT cells were 3D printed and cell viability and biological functions were studied. Parameters, i.e. matrix material composition, chamber temperature, nozzle temperature were optimized to achieve high cellular viability after printing. As shown in figure 2(a), embedding 293FT cells in matrix materials by manual mixing and keeping the mixture at 4, 25, and 37 °C for 10–30 min did not lead to obvious cell death. Manual extrusion at room temperature after blending could keep about 95% cells

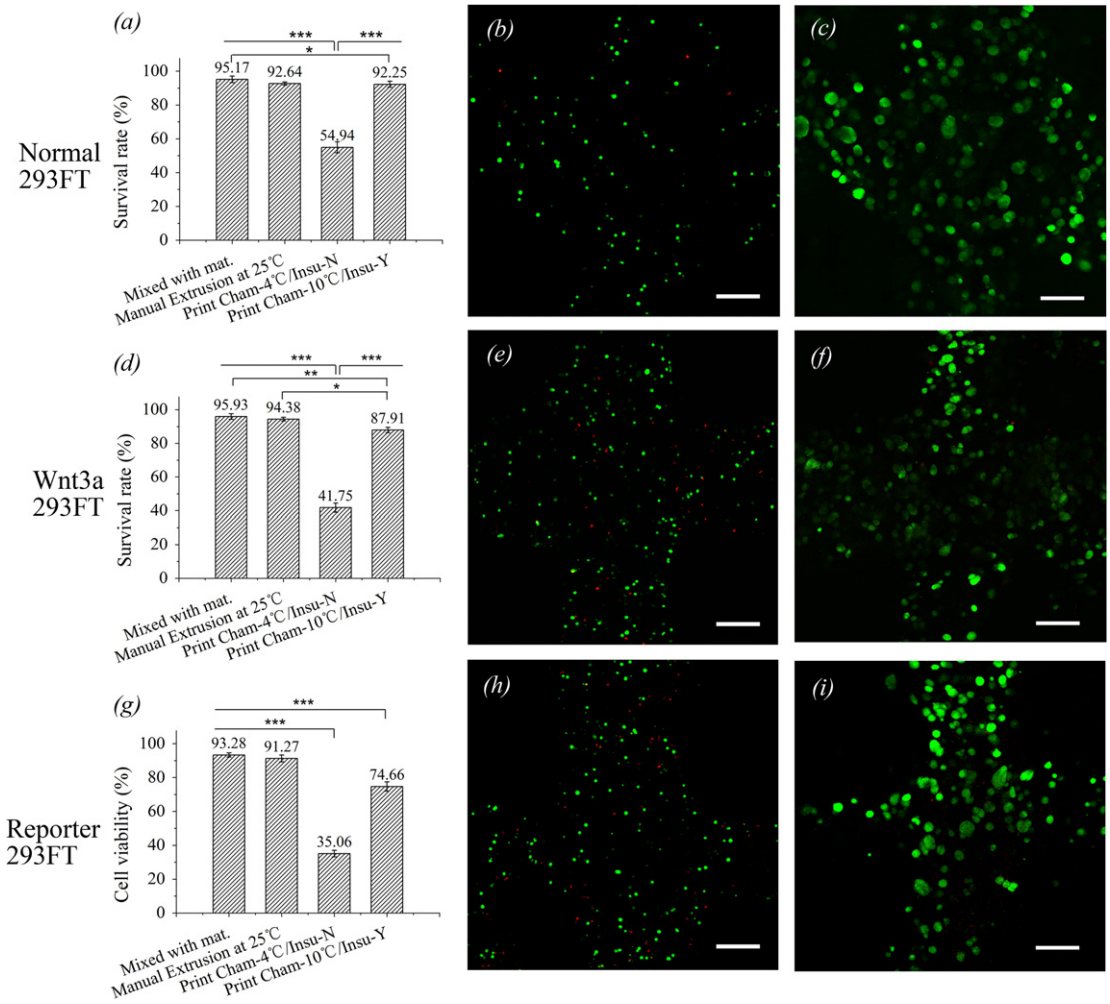

Figure 3. Process optimization to improve cell viability. (a), (d) and (g) Quantitative analysis of cell viability right after printing under different conditions (a) normal 293FT, (d) Wnt3a-293FT and (g) Wnt reporter-293FT. (b), (e) and (h) Live/dead staining images for the three kinds of cells at day 0. (c), (h) and (i) Live/dead staining images for the three kinds of cells at day 3. Cham-4/10 °C means setting the chamber temperature at 4 OR 10 °C. Insu-Y/N means with OR without insulation for nozzle at 25 °C. All these results were based on gelatin/alginate materials. Scale: 200 μm.

alive ((95.17 ± 1.926), (95.93 ± 1.652) and (93.28 ± 1.217)% for HEK 293FT, Wnt3a-293FT and Wnt reporter-293FT, respectively, without significant differences). However, during the 3D bioprinting process, chamber temperature and nozzle temperature showed significant impact on cell viability. When the chamber temperature was set at 4 °C (cham-4 °C) without nozzle insulation (Insu-N), the viability of HEK 293FT cells after 3D printing was only (54.94 ± 3.264) and (55.14 ± 1.719)% for G–A group and G–A–F group (figure 2(b)), respectively, without significant difference. When the chamber temperature was set at 10 °C (cham-10 °C) with nozzle insulation at 25 °C (Insu-Y), the viability of HEK 293FT cells increased to (92.25 ± 1.813) and (90.77 ± 1.498)% for G–A group and G–A–F group (figure 2(b)), respectively, without significant differences.

Using the same parameters as HEK 293FT (figures 3(a), (b)), other two types of cells were printed applying G–A materials group. Compared with cham-4 °C/Insu-N condition, the viability of cham-10 °C/Insu-Y condition increased significantly from (41.75 ± 2.743) to (87.91 ± 1.609)% and from (35.06 ± 1.907) to (74.66 ± 2.798)% for Wnt3a-293FT and Wnt reporter-293FT (figures 3(d), (e), (g) and (h)), respectively. The viability of both Wnt3a-293FT and Wnt reporter-293FT under optimized condition was less than that HEK 293FT. However, few cells were found dead after 3 days culture for all three groups (figures 3(c), (f) and (i)).

3.2. Structural characteristic of the cell-laden constructs

The structural characteristic and long-term stability of cell-laden constructs was studied in this research. As shown in figures 4(a) and (b), both G–A and G–A–F constructs showed clear grid structure after 3D printing using same parameters mentioned above. Due to chemical crosslinking of alginate by $CaCl_2$ solution, the overall size of the G–A construct shrunk to about 97.45% of the designed size. Under the current parameter setting, the thread diameter of the G–A

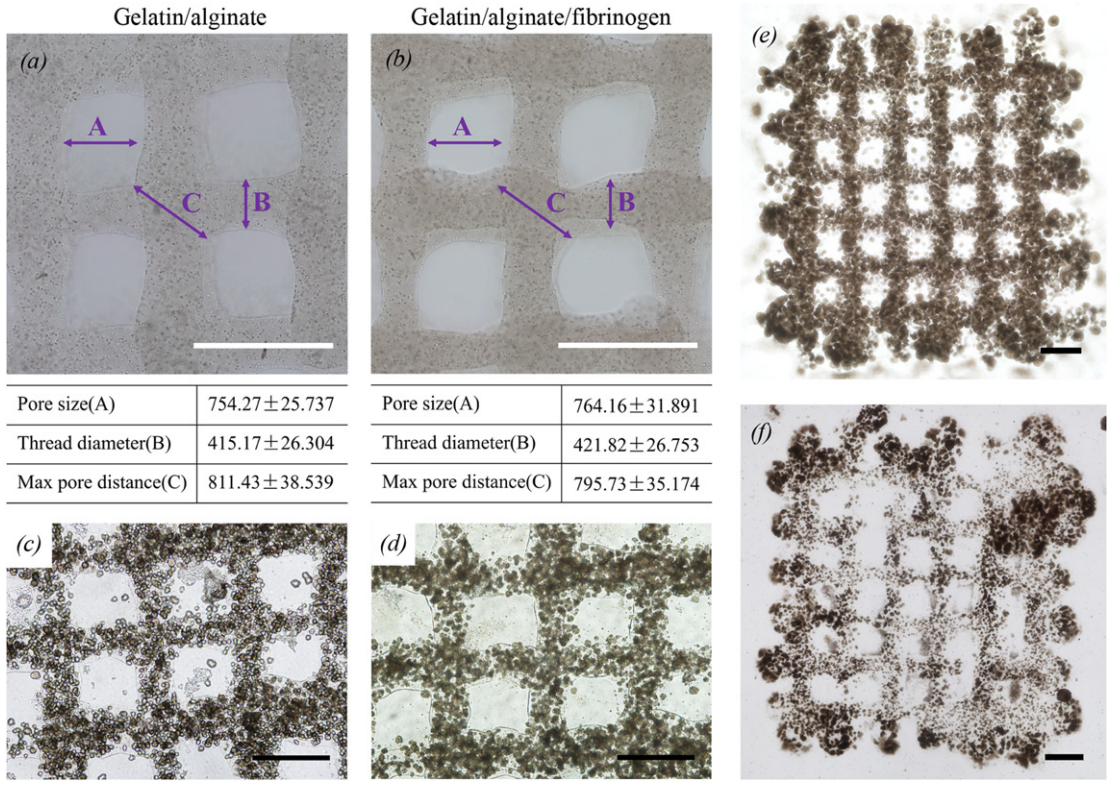

Pore size(A)	754.27±25.737
Thread diameter(B)	415.17±26.304
Max pore distance(C)	811.43±38.539

Pore size(A)	764.16±31.891
Thread diameter(B)	421.82±26.753
Max pore distance(C)	795.73±35.174

Figure 4. Gel material comparison and 3D construct stability over time. (a) and (b) The construct configuration of G–A (a) and G–A–F (b) material groups after printing at day 0. (c) and (d) Bright field images of G–A (c) and G–A–F (d) material groups after culturing for nine days. (e) and (f) The construct integrity and cell condition at day 14 (e) and day 30 (f) for the G–A group. All the above results were based on HEK 293FT cells. Scale: 1 mm.

construct was 415.17 ± 26.304 μm (figure 4(a)), which was 1.60 times of the inner diameter of the printing nozzle (260 μm). On the other hand, because of crosslinking of alginate by $CaCl_2$ and crosslinking of fibrinogen by thrombin, the overall size of the G–A–F construct was about 98.83% of the designed size, with the thread diameter of about 1.62 times to the inner diameter of the printing nozzle (figure 4(b)).

After 9 days of culture, the constructs of both material groups maintained the integrity and uniform cell aggregates began to fill the threads (figures 4(c) and (d)). The density of cells in gels increased over time. By 14 days, above 90% space was filled by cell aggregates with diameter around hundred-microns, while the constructs still maintained the integrity with clear grid structure (figure 4(e)). In fact, the structure stayed stable for more than 30 days as long as it attached to the bottom of the petri dish rather than floating in the medium (figure 4(f)). However, after 30 days of continuous culture, cell quality and viability declined possibly due to contact inhibition and insufficient oxygen and nutrient diffusion into the large cellular spheroids in the 3D structure (figure 4(f)).

3.3. Morphological change in 3D construct

Cell aggregates were formed within gels and the aggregate growth was monitored during culturing. Figure 5 clearly showed the growth of cell aggregates from several cells at day 2 to dozens of cells at day 5. Cell proliferation was evident from both the bright field and fluorescence images. All the assays conducted in this study were within one week, during which time the aggregate wouldn't be too large to restrict the inner cells.

3.4. Cell proliferation in 3D construct compared with 2D culture

Growing in aggregates, cell proliferation in 3D can be evaluated through measuring the diameter of cell aggregates (figure 6(a)). Cell proliferation was quantified using CCK-8 assay and showed in figure 6(b): dramatic increase in cell growth was observed from day 1 to day 5, while after 5 days, the increment slowed down. Based on CCK-8 assay, cells in 2D condition showed faster proliferation, especially after day 3.

However, figure 6(c) presents the normalized data of 2D OD and 3D volume, which both reflected the cell quantity. The results demonstrated that 3D aggregates turned to be an exponential growth, which grew faster than 2D, especially after day 5.

3.5. Cellular function of Wnt-293FT and Wnt reporter-293FT

Western blot was used to investigate whether protein expression from cells grown in 3D constructs was similar with that from 2D cultured cells. The results showed that Wnt3a protein was synthesized by

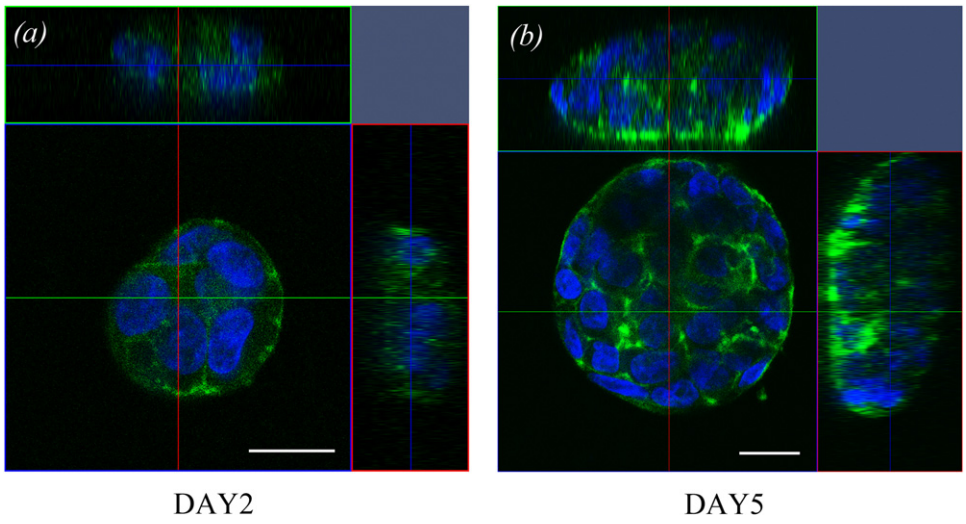

Figure 5. Cell aggregate morphology. Cell aggregate grew from several cells to dozens of cells, respectively from day 2 to day 5. Scale: 20 μm.

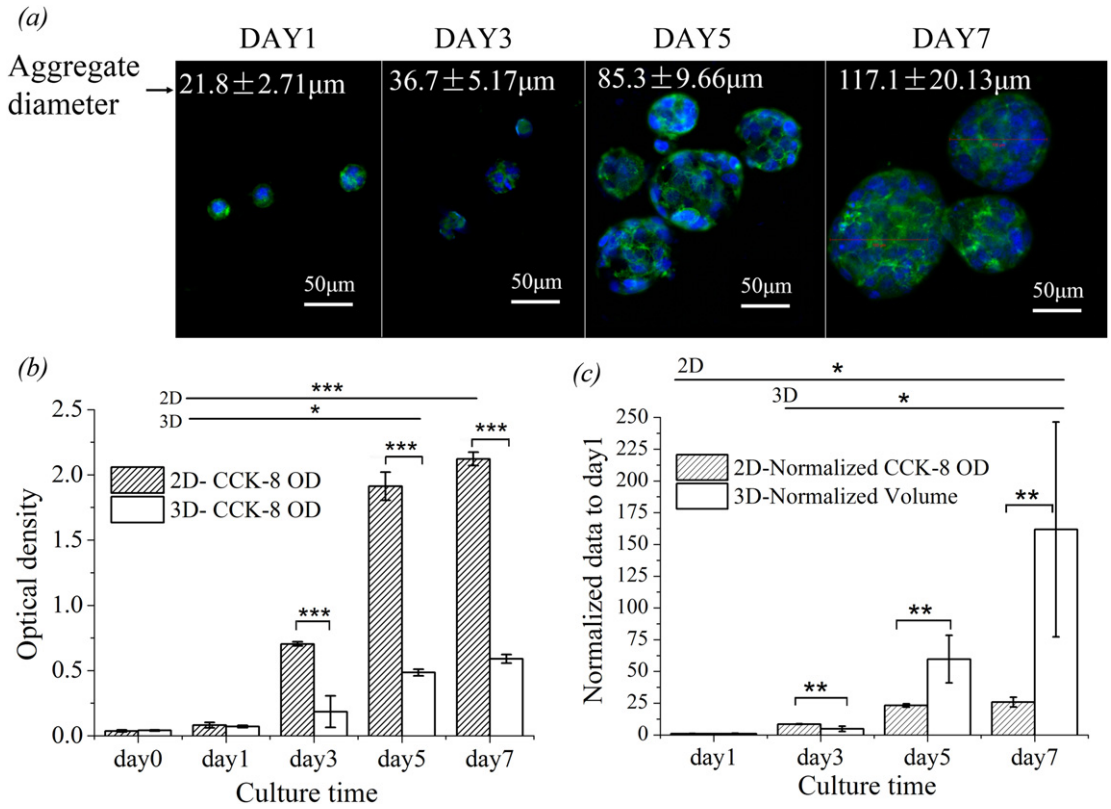

Figure 6. Cell proliferation in 2D and 3D conditions. (a) Cell aggregates in 3D condition grew with the culture time. The aggregate diameter was shown as mean ± SD in each image ($n = 13$). (b) Optical density (OD) value for 2D and 3D conditions using CCK-8 kit. (c) Cell proliferation rate after normalized to OD value of day 1 and aggregate volume for 2D and 3D, respectively.

Wnt3a-293FT cells embedded in gels. Figure 7(a) showed the obvious band of Wnt3a and housekeeping gene GAPDH. Interestingly, after normalization against the protein level GAPDH, there seemed to be more Wnt3a protein expressed by 3D cultured cells compared to 2D cultured cells (Wnt3a-3D/GAPDH = 0.42 ± 0.124 versus Wnt3a-2D/GAPDH = 0.28 ± 0.052, figure 7(b)).

For tissue fabrication using 3D bioprinting technology, it is essential that cells in 3D constructs can respond to external signals. To test this, we used Wnt reporter-293FT cells. These cells were genetically engineered to carry a mCherry fluorescent protein reporter. Upon receiving stimulus to activate Wnt signaling pathway, the reporter will be turned on and cells will express mCherry and display red fluorescence. As we expected, upon addition of small molecule Wnt

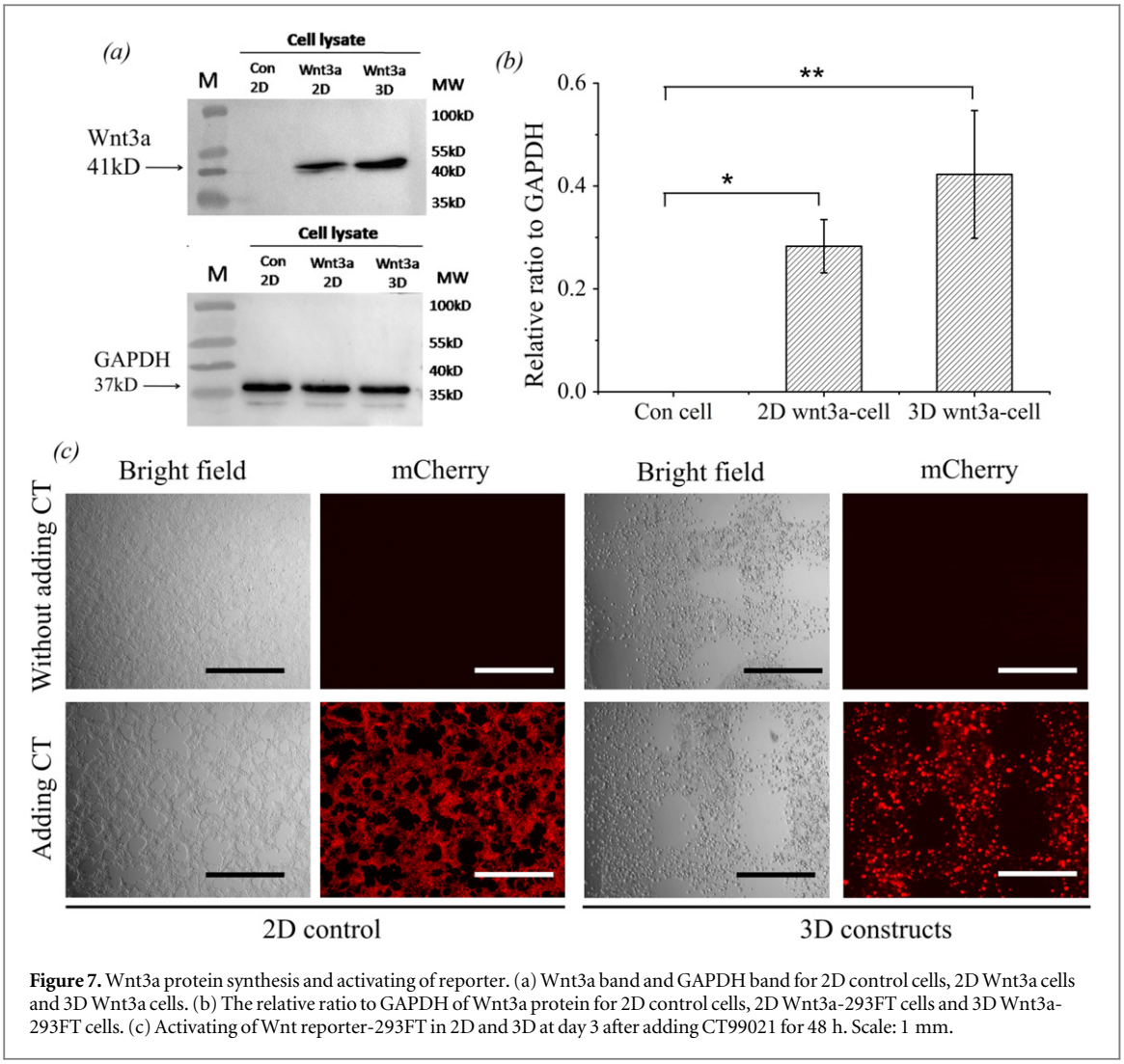

Figure 7. Wnt3a protein synthesis and activating of reporter. (a) Wnt3a band and GAPDH band for 2D control cells, 2D Wnt3a cells and 3D Wnt3a cells. (b) The relative ratio to GAPDH of Wnt3a protein for 2D control cells, 2D Wnt3a-293FT cells and 3D Wnt3a-293FT cells. (c) Activating of Wnt reporter-293FT in 2D and 3D at day 3 after adding CT99021 for 48 h. Scale: 1 mm.

signaling pathway activator CT99021, Wnt reporter-293FT cells showed bright red fluorescence comparable to reporter cells in 2D environment treated with CT99021 (figure 7(c)). Thus, cells grown in gel structure following 3D printing could receive chemical stimulus and had normal cell signaling function.

4. Discussion

In this study, we optimized 3D bioprinting conditions for HEK 293FT cells, characterized their viability, proliferation and morphology during long-term culture in 3D gel structure. Moreover, the results showed that our 3D bioprinted cells had normal protein expression and can activate Wnt signaling pathway in 3D environment upon chemical stimulus. The G–A mixture had been used to print hepatocyte and ADSCs for some tissue engineering applications [31, 42], and G–A–F materials were also used to print ADSCs to guide multipotent differentiation towards adipocyte and endothelial cells [30]. In our experiments, we found that 3D constructs with both G–A and G–A–F matrix biomaterials could maintain long-term stability (figure 4) and high cell viability with little differences (figure 2(b)), while with one more bioactive material and crosslinking process, the G–A–F system suffered from more complex operations and variables. Cells in G–A constructs grew as cell aggregates and filled 90% space of the construct after two weeks of culture with the initial concentration of 2×10^6 cells/mL. Therefore, as a simpler material system, the G–A group was chosen for all later experiments to study the influences of other factors. Based on the G–A materials, a homogeneous 3D grid was designed and fabricated. Because of the swelling of hydrogels after extruded from nozzle, the thread size became wider than the inner diameter of the nozzle. The average thread width of $415.17 \pm 26.304\ \mu$m was sufficient for cell growth, as cells could distribute evenly throughout the whole construct.

It is crucial to preserve cell viability and normal biological function after biofabrication process and construct formation [43–46]. Previous studies showed that the printing process caused little damage to cells for the subsequent studies [46, 47]. However, this could be cell type and printing technology dependent. More specifically, stimulation sources from laser

energy, bubble breakup, impulsive force are addressed in laser directed writing, laser-induced forward printing, inkjet printing, valve-based printing respectively [48–50]. As for the extrusion printing, shear force was generally responsible for most of the cell damage [43].

Applying the previous printing condition (cham-4 °C, Insu-N), viability decrease was observed during the whole process, and a dramatic reduction existed from manual extraction at RT to real printing (figures 3(a), (d) and (g)). Though the whole printing process for 1 mL cell/material mixture would last about 30 min, during which time unprinted cells lacked culture medium at a relatively low temperature, the results in figure 2(a) excluded the influence of staying at different temperature (4, 25 and 37 °C) within 30 min on cell viability. So, it was believed that the high shear force on cells in the nozzle was the main reason for low viability, apart from cell type changing [43]. Shear force caused by surrounding materials was mostly determined by the viscosity or gelation degree of hydrogels [51]. As a temperature-sensitive hydrogel, the viscosity of gelatin changed sharply with temperature, especially around the gelation region, which was also utilized to print real 3D structures by the adopted machine [52]. Higher viscosity gives better structure quantity but compromises cell viability [44, 53]. This promoted us to reduce the shear force by increasing the printing temperature to improve cell viability while stable 3D structure could be fabricated. In fact, the adoption of higher temperature in printing chamber and thermo insulation in the nozzle indeed improved the viability of HEK 293FT cells significantly from (54.94 ± 3.264) to $(92.25 \pm 1.813)\%$. However, differences on viability were observed when printing the genetically engineered HEK 293 cell using the modified process parameters. In general, HEK 293FT cells showed the highest viability, followed by Wnt3a-293FT stable line $(87.90 \pm 1.609)\%$, and then Wnt reporter line $(74.66 \pm 2.798)\%$. It was possible that certain transgenic cell lines were more sensitive than the parental line, which might explain their decreased viability. Nonetheless, few dead cells were observed after 1 day of culture for all three groups, suggesting that the debris of dead cells spontaneously dissolved during culture.

The hydrogel constructs provided a 3D microenvironment resembling the *in vivo* environment for a range of cellular activities such as cell growth and cytokine signal transduction. Unlike the 2D culture, 293FT cells grew as aggregates in gelatin/alginate hybrid materials. The cell aggregates not only reflected active cell proliferation, but also represent different cell–cell interaction in 3D gel structure [54]. Based on CCK-8 assay, cell aggregates in gels seemed to have slower proliferation rate compared with 2D cultured cells. However, the normalized cell aggregate volume turned to grow faster than normalized OD value of 2D cultured cells. The CCK-8 cell proliferation quantification kit was normally used for 2D cultured cells and may not be able to accurately reflect cell proliferation in 3D culture. As shown in our results, 3D cultured HEK293FT cells grew to large spheroids, thus the inside cells may not be exposed to the WST-8 substrate. The crosslinked hydrogels may also reduce the diffusion of chemicals. Consequently, WST-8 in CCK-8 solution may not react to all cells in 3D constructs, which lead to lower OD value. Interestingly, more Wnt3a protein was made by cells grew in 3D constructs, which suggests that cell shape may influence protein synthesis. Moreover, despite that cells were in very different shape, Wnt reporter cells still responded to chemical signals and turned on mCherry expression. These results proved that our 3D bioprinted cells have normal biological function, cell signaling activity and gene transcription response.

5. Conclusion

In this study, we successfully printed HEK 293FT cells and two genetically engineered cell lines with high viability using a 3D hydrogel bioprinter. We found that the shear force seemed to be the major cause of cell death during printing and increasing temperature could effectively reduce the viscosity of the hydrogel and improve cell survival after printing. During prolonged culture, cells grew as spheroids in the 3D constructs, and cellular spheroids-gel integrity was maintained for over four weeks. Cell proliferation rate, cell shape and interactions and protein synthesis were different in 3D gel environment and standard 2D culture conditions. In summary, the current work about 3D bioprinting of HEK 293FT cells using a hydrogel extrusion printer form the basis for using this platform to print different types of embryonic cells and study tissue interactions. It is an important step forward toward biofabrication of mammalian tissues with 3D printing technology.

Acknowledgments

The authors acknowledge the funding supports from the National Natural Science Foundation of China through project No. 51235006, the National High Technology Research and Development Program of China (863 Program) through project No. 2012AA020506 and the Shenzhen Development and Reform Commission. This work was also supported by the National Natural Science Foundation of China Grant 31171381 and the National Basic Research Program of China, 973 program grant 2012CB966701 to (J.N.), and the funding of the Tsinghua-Peking Center for Life Sciences.

References

[1] Calvert P 2007 Materials science. Printing cells *Science* **318** 208–9

[2] Tasoglu S and Demirci U 2013 Bioprinting for stem cell research *Trends Biotechnol.* **31** 10–9

[3] Birgersdotter A, Sandberg R and Ernberg I 2005 Gene expression perturbation *in vitro*—a growing case for three-

dimensional (3D) culture systems *Semin. Cancer Biol.* **15** 405–12
[4] Yao R, Du Y, Zhang R, Lin F and Luan J 2013 A biomimetic physiological model for human adipose tissue by adipocytes and endothelial cell cocultures with spatially controlled distribution *Biomed. Mater.* **8** 045005
[5] Dickinson L E, Lutgebaucks C, Lewis D M and Gerecht S 2012 Patterning microscale extracellular matrices to study endothelial and cancer cell interactions *in vitro Lab Chip* **12** 4244–8
[6] Gruene M *et al* 2011 Laser printing of three-dimensional multicellular arrays for studies of cell–cell and cell–environment interactions *Tissue Eng. C: Methods* **17** 973–82
[7] Lutolf M P, Gilbert P M and Blau H M 2009 Designing materials to direct stem-cell fate *Nature* **462** 433–41
[8] Guilak F, Cohen D M, Estes B T, Gimble J M, Liedtke W and Chen C S 2009 Control of stem cell fate by physical interactions with the extracellular matrix *Cell Stem Cell* **5** 17–26
[9] Yao R, Zhang R, Luan J and Lin F 2012 Alginate and alginate/gelatin microspheres for human adipose-derived stem cell encapsulation and differentiation *Biofabrication* **4** 025007
[10] Gaebel R *et al* 2011 Patterning human stem cells and endothelial cells with laser printing for cardiac regeneration *Biomaterials* **32** 9218–30
[11] Xu T, Zhao W, Zhu J M, Albanna M Z, Yoo J J and Atala A 2013 Complex heterogeneous tissue constructs containing multiple cell types prepared by inkjet printing technology *Biomaterials* **34** 130–9
[12] Fedorovich N E, Alblas J, Hennink W E, Oner FC and Dhert W J 2011 Organ printing: the future of bone regeneration? *Trends Biotechnol.* **29** 601–6
[13] Chang R, Emami K and Wu H 2010 Biofabrication of a three-dimensional liver micro-organ as an *in vitro* drug metabolism model *Biofabrication* **2** 045004
[14] Chang R, Nam J and Sun W 2008 Direct cell writing of 3D microorgan for *in vitro* pharmacokinetic model *Tissue Eng. C: Methods* **14** 157–66
[15] Xu F, Wu J, Wang S, Durmus N G, Gurkan U A and Demirci U 2011 Microengineering methods for cell-based microarrays and high-throughput drug-screening applications *Biofabrication* **3** 034101
[16] Rodriguez-Devora J I, Zhang B, Reyna D, Shi Z D and Xu T 2012 High throughput miniature drug-screening platform using bioprinting technology *Biofabrication* **4** 035001
[17] Gruene M, Deiwick A, Koch L, Schlie S, Unger C, Hofmann N, Bernemann I, Glasmacher B and Chichkov B 2011 Laser printing of stem cells for biofabrication of scaffold-free autologous grafts *Tissue Eng. C: Methods* **17** 79–87
[18] Khatiwala C, Law R, Shepherd B, Dorfman S and Csete M 2012 3D cell bioprinting for regenerative medicine research and therapies *Gene Ther. Reg.* **7** 1230004
[19] Mironov V, Kasyanov V and Markwald R R 2011 Organ printing: from bioprinter to organ biofabrication line *Curr. Opin. Biotechnol.* **22** 667–73
[20] Nahmias Y, Schwartz R E, Verfaillie C M and Odde D J 2005 Laser-guided direct writing for three-dimensional tissue engineering *Biotechnol. Bioeng.* **92** 129–36
[21] Colina M, Duocastella M, Fernández-Pradas J M, Serra P and Morenza J L 2006 Laser-induced forward transfer of liquids: study of the droplet ejection process *J. Appl. Phys.* **99** 084909
[22] Boland T, Xu T, Damon B and Cui X 2006 Application of inkjet printing to tissue engineering *Biotechnol. J.* **1** 910–7
[23] Nakamura M *et al* 2005 biocompatible inkjet printing technique for designed seeding of individual living cells *Tissue Eng.* **11** 1658–66
[24] Yan Y *et al* 2005 Fabrication of viable tissue-engineered constructs with 3D cell-assembly technique *Biomaterials* **26** 5864–71
[25] Demirci U and Montesano G 2007 Cell encapsulating droplet vitrification *Lab Chip* **7** 1428–33
[26] Demirci U and Montesano G 2007 Single cell epitaxy by acoustic picoliter droplets *Lab Chip* **7** 1139–45
[27] Zhao Y, Yao R, Ouyang L, Ding H, Zhang T, Zhang K, Cheng S and Sun W 2014 Three-dimensional printing of Hela cells for cervical tumor model *in vitro Biofabrication* **6** 035001
[28] Ilkhanizadeh S, Teixeira A I and Hermanson O 2007 Inkjet printing of macromolecules on hydrogels to steer neural stem cell differentiation *Biomaterials* **28** 3936–43
[29] Koch L *et al* 2010 Laser printing of skin cells and human stem cells *Tissue Eng. C: Methods* **16** 847–54
[30] Xu M, Wang X, Yan Y, Yao R and Ge Y 2010 An cell-assembly derived physiological 3D model of the metabolic syndrome, based on adipose-derived stromal cells and a gelatin/alginate/fibrinogen matrix *Biomaterials* **31** 3868–77
[31] Yao R, Zhang R J, Yan Y N and Wang X H 2009 *In vitro* angiogenesis of 3D tissue engineered adipose tissue *J. Bioact. Compat. Polym.* **24** 5–24
[32] Gaetani R, Doevendans P A, Metz C H G, Alblas J, Messina E, Giacomello A and Sluijtera J P G 2012 Cardiac tissue engineering using tissue printing technology and human cardiac progenitor cells *Biomaterials* **33** 1782–90
[33] Gaetani R, Feyen D, Verhage V, Slaats R, Messina E, Giacomello A, Doevendans P and Sluijter J 2012 Tissue-Printed cardiac progenitor cells improve myocardial function in a mouse model of MI *Circ. Res.* **111** A345
[34] Matsusaki M, Sakaue K, Kadowaki K and Akashi M 2013 Three-dimensional human tissue chips fabricated by rapid and automatic inkjet cell printing *Adv. Healthc. Mater.* **2** 534–9
[35] Faulkner-Jones A, Greenhough S, King J A, Gardner J, Courtney A and Shu W 2013 Development of a valve-based cell printer for the formation of human embryonic stem cell spheroid aggregates *Biofabrication* **5** 015013
[36] Lee W, Pinckney J, Lee V, Lee J H, Fischer K, Polio S, Park J K and Yoo S S 2009 Three-dimensional bioprinting of rat embryonic neural cells *Neuroreport* **20** 798–803
[37] Shen C F and Kamen A 2012 Hyperosmotic pressure on HEK 293 cells during the growth phase, but not the production phase, improves adenovirus production *J. Biotechnol.* **157** 228–36
[38] McConnell M P, Dhars S, Naran S, Nguyen T, Bradshaw R and Evans G R D 2004 *In vivo* induction and delivery of nerve growth factor, using HEK-293 cells *Tissue Eng.* **10** 1492–501
[39] Peifer M and Polakis P 2000 Cancer—Wnt signaling in oncogenesis and embryogenesis—a look outside the nucleus *Science* **287** 1606–9
[40] Augst A D, Kong H J and Mooney D J 2006 Alginate hydrogels as biomaterials *Macromol. Biosci.* **6** 623–33
[41] Marucco A, Fenoglio I, Turci F and Fubini B. 2013 Interaction of fibrinogen and albumin with titanium dioxide nanoparticles of different crystalline phases *J. Phys.: Conf. Ser.* 429
[42] Liu H X, Li S J and Yan Y N 2011 Cell direct assembly technology adopting hybrid of gelatin-based hydrogels *Adv. Mater. Res.* **189-193** 2986–92
[43] Nair K, Gandhi M, Khalil S, Yan K C, Marcolongo M, Barbee K and Sun W 2009 Characterization of cell viability during bioprinting processes *Biotechnol. J.* **4** 1168–77
[44] Yu Y, Zhang Y, Martin J A and Ozbolat I T 2013 Evaluation of cell viability and functionality in vessel-like bioprintable cell-laden tubular channels *J. Biomech. Eng.* **135** 91011–9
[45] Yan K C, Nair K and Sun W 2010 Three dimensional multi-scale modelling and analysis of cell damage in cell-encapsulated alginate constructs *J. Biomech.* **43** 1031–8
[46] Jakab K, Norotte C, Marga F, Murphy K, Vunjak-Novakovic G and Forgacs G 2010 Tissue engineering by self-assembly and bioprinting of living cells *Biofabrication* **2** 022001
[47] Ferris C J, Gilmore K G, Wallace G G and In Het Panhuis M 2013 Biofabrication: an overview of the approaches used for printing of living cells *Appl. Microbiology Biotechnol.* **97** 4243–58
[48] Barron J A, Krizman D B and Ringeisen B R 2005 Laser printing of single cells: statistical analysis, cell viability, and stress *Ann. Biomed. Eng.* **33** 121–30
[49] Cui X, Dean D, Ruggeri Z M and Boland T 2010 Cell damage evaluation of thermal inkjet printed chinese hamster ovary cells *Biotechnol. Bioeng.* **106** 963–9
[50] Tirella A, Vozzi F, De Maria C, Vozzi G, Sandri T, Sassano D, Cognolato L and Ahluwalia A 2011 Substrate stiffness influences high resolution printing of living cells with an ink-jet system *J. Biosci. Bioeng.* **112** 79–85

[51] Yan C, Mackay M E, Czymmek K, Nagarkar R P, Schneider J P and Pochan D J 2012 Injectable solid peptide hydrogel as a cell carrier: effects of shear flow on hydrogels and cell payload langmuir *ACS J. Surf. Colloids* **28** 6076–87
[52] Liu H X, Li S J and Yan Y N 2011 Cell direct assembly technology adopting hybrid of gelatin-based hydrogels *Manuf. Process Technol.* **189-193** 2986–92
[53] Yusof A, Keegan H, Spillane C D, Sheils O M, Martin C M, O'Leary J J, Zengerle R and Koltay P 2011 Inkjet-like printing of single-cells *Lab Chip* **11** 2447–54
[54] Loessner D, Stok K S, Lutolf M P, Hutmacher D W, Clements J A and Rizzi S C 2010 Bioengineered 3D platform to explore cell–ECM interactions and drug resistance of epithelial ovarian cancer cells *Biomaterials* **31** 8494–506